Lab on a Chip

Devices and applications at the micro- and nanoscale

Accepted Manuscript

This article can be cited before page numbers have been issued, to do this please use: Z. Zhang, M. Azizi, M. Lee, P. Davidowsky, P. Lawrence and A. Abbaspourrad, *Lab Chip*, 2019, DOI: 10.1039/C9LC00734B.

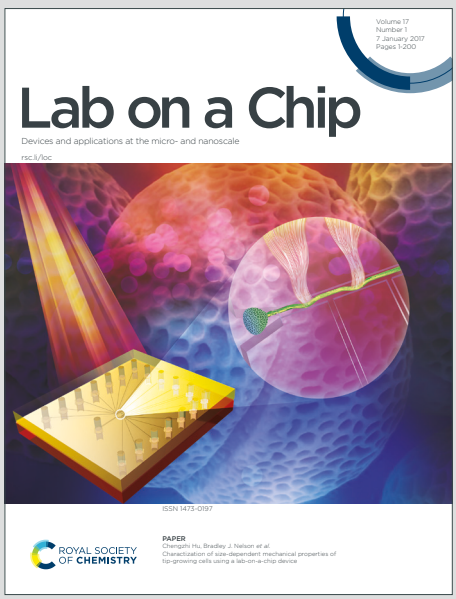

ROYAL SOCIETY OF CHEMISTRY

rsc.li/loc

A versatile, cost-effective, and flexible wearable biosensor for *in situ* and *ex situ* sweat analysis, and personalized nutrition assessment

Zhong Zhang, Morteza Azizi, Michelle Lee, Philip Davidowsky, Peter Lawrence, Alireza Abbaspourrad*

Department of Food Science, College of Agriculture and Life Sciences, Cornell University, Ithaca 14853, NY, USA

***Correspondence**: Alireza Abbaspourrad, Department of Food Science, College of Agriculture and Life Sciences, Cornell University, Ithaca 14853, NY, USA. Tel: (607) 255-2923. Email: Alireza@cornell.edu

Abstract: Point-of-care (POC) diagnostics have shown excellent potential in rapid biological analysis and health/disease monitoring. Here, we introduce a versatile, cost-effective, flexible, and wearable POC biomarker patch for effective sweat collection and health monitoring. We design and fabricate channels/patterns on filter paper using wax printing technology, which can direct sweat to collection and biomarker detection zones on the proposed platform. The detection zones are designed to measure the amount of collected sweat, in addition to measuring the sweat pH, and glucose (a potential diabetic biomarker), and lactate concentrations. It is significantly challenging to measure glucose in human sweat by colorimetric methods due to the extremely low glucose levels found in this medium. However, we overcame this issue by effectively engineering our wearable biosensor for optimal intake, storage, and evaporation of sweat. Our design concentrates the colorant (indicator) into a small detection zone and significantly increases the sensitivity for the sweat glucose sensing reactions. The device can thus detect glucose in physiological glucose concentration range of 50–300 μM. This cost-effective and wearable biosensor can provide instant *in situ* quantitative results for targets of interests, such as glucose, pH, and lactate, when coupled with the imaging and computing functionalities of smartphones. Meanwhile, it is also feasible to extract the air-dried sweat from the storage zone for further *ex situ* measurements of a broader portfolio of biomarkers, leading to applications of our wearable biosensor in personalized nutrition and medicine.

Keywords: wearable biosensors, point-of-care, sweat collection, biomarker detection, glucose, lactate, personalized nutrition.

Introduction: Human sweat, the transparent fluid secreted by sweat glands in the skin, contains rich healthcare information regarding human metabolism and physiological status[1-8]. The maximum sweat rates of an adult can be up to 2–4 liters per hour (10–15 g/min·m^2)[9-11]. This abundant biofluid contains electrolytes (*e.g.*, sodium and potassium), metabolites (*e.g.*, lactate and pyruvate), nitrogenous substances (*e.g.*, amino acids and proteins), nutrients (*e.g.*, glucose and vitamins), and various disease biomarkers[12-17]. Quantification of biomolecules in human sweat can provide insightful information for the diagnosis of disease, tracking of physiological health, and monitoring nutritional balance[18-21]. Despite the rich information contained in sweat and the non-invasive nature of sweat collection, the lack of cost-effective and convenient sampling devices for the collection and storage of this material has limited its versatility for biomonitoring applications[22, 23]. Wearable point-of-care (POC) devices may serve a potential solution to this challenge, providing simultaneous sampling and monitoring of target molecules found in sweat, such as glucose, lactate, and measuring the pH[16, 24-28]. An ideal wearable POC platform should be lightweight, comfortable, flexible, and sensitive to the target biomolecule detection[29, 30]. Most importantly, it must be cost-effective to fabricate[31, 32].

Glucose, lactate, and minerals are often selected as targets of interests due to their relation with disease state, physiological metabolism, and hydration status[3, 33, 34]. Recently, studies have demonstrated *in situ* measurements of such biomolecules with some success using wearable biosensors featuring biosensor parts directly in contact with human skin for electrochemical or colorimetric sensing[6, 35, 36]. Electrochemical sensors have many advantages, such as high sensitivity, real-time measurement, and easy adaption for wireless data transfer, though the disadvantages include the high-cost

associated with the fabrication of the digital components, the low flexibility of the biosensor, and the physical discomfort on human skin[37, 38]. In addition, current electrochemical, wearable biosensors lack the ability to conveniently store and transport sweat for further analysis in the lab (*i.e.* further *ex situ* analyses)[6, 39]. A convenient and light-weight sweat storage design is especially useful for the analysis and would provide a new path to non-invasively monitor human nutrition, opening a window to personalized nutrition/medicine.

Recently, researchers fabricated microfluidic devices consisting of polydimethylsiloxane (PDMS) for the capture, storage, and colorimetric sensing of sweat[35, 40]. One major challenge of colorimetric sensing is the difficulty in measuring biomolecules that are typically found in low concentrations in sweat, such as glucose[35, 36, 41]. The normal glucose level in human sweat is estimated between 50–120 μM by an electrochemical sensor. The concentration, 50 μM, is the low end of the normal range, while 120 μM or higher may indicate potentially high blood glucose levels[6]. To the best of our knowledge, no report has demonstrated the ability to cover the linear range of 50 to 120 μM of glucose on a wearable device using an optical/colorimetric readout. In addition, it is still difficult to scale-up the process for making PDMS-based microfluidic biosensors due to the labor-intensive and time-consuming process[42].

Herein, we demonstrate a versatile, cost-effective, flexible, wearable biosensor using regular filter paper and medical tapes. The channels/patterns were designed and printed on the paper using a wax printer. These channels then direct the sweat to collection and detection zones of the device, where the intake, storage, and evaporation of sweat is engineered to maximize the efficiency of the colorimetric sensing reactions, leading to a high sensitivity for the measurement of glucose. The wearable patch can provide

facile, visual readouts for the targets when coupled with the imaging and computing functionalities of a smartphone. After the collected sweat is air-dried in the patch, it can be easily stored at room temperature and also sent to a laboratory for further *ex situ* analysis of nutrition and disease biomarkers, enabling personalized nutrition and medicine. Subsequently, we have demonstrated the use of this versatile, cost-effective, and flexible POC patch to monitor glucose, pH, and sweat loss using both simulated artificial and real collected sweat from human subjects.

Materials and Methods

Materials and chemicals

Glucose oxidase (G6125-10KU), lactate oxidase (L9795-50UN), peroxidase (P8375-1KU), sodium 3,5-dichloro-2-hydroxybenzenesulfonate (DHBS), 4-aminoantipyrine (AAP), o-phenylenediamine, potassium iodide, 3,3′,5,5′-tetramethylbenzidine (TMB), chitosan, glucose (> 98%), sodium hydroxide, sodium phosphate dibasic, sodium phosphate monobasic, lactic acid, urea, hydrogen chloride, ammonium chloride, and sodium chloride were purchased from Sigma-Aldrich (St Louis, MO, USA) and used without any purification. Trehalose was purchased from TCI chemicals (TCI America, Portland, OR, USA). The universal pH indicator, Bogens in alcohol, is from LabChem (Zelienople, PA, USA). Whatman qualitative filter paper (#1) was used in the study. A Xerox Phaser 8200 solid ink printer (Norwalk, CT, USA) was used to print the biosensing patterns on the filter paper. Ultrapure water (18.2 MΩ/cm) was prepared from a Millipore water purification system (Burlington, MA, USA).

Fabrication of the wearable patch

The Autodesk Inventor and Microsoft PowerPoint software were used to design the

patterns. The line width on the PowerPoint file was set to 1.81 points (**Fig. S1**). The pattern was printed on a piece of filter paper mounted on A-4 paper using the solid ink printer. The printed wax ink was melted by placing the filter paper on a hot plate (170 ^{o}C) for 180 s. The melted wax penetrated through the filter paper, creating hydrophobic barriers in the otherwise hydrophilic cellulose substrate, leading to the formation of channels within the filter paper.[43-45] The sensing chemicals were loaded and dried on the designated zones on the filter paper before being sealed by medical tape. Transparent, single-sided and double-sided medical tape (1522, 1526) was provided by 3M (Maplewood, MN, USA). The inlets and outlets/vents for the sweat were created on the medical tape using a metal punch with adjustable punching sizes (**Fig. S2**).

Detection of glucose, lactate, pH, and sweat loss

For glucose detection, we cast glucose oxidase solution (3.5 mg/mL, 4.0 μL, pH 6.1 phosphate buffer), horseradish peroxidase (0.1 mg/mL, 4.0 μL, pH 6.1 buffer), and AAP/DHBS solution (4.0 μL, 4 mM / 8 mM) on the glucose detection zone in sequence and air-dried. The lactate measurement was similarly achieved using *L*-lactate oxidase (4.0 μL, 2 mg/mL), horseradish peroxidase (4.0 μL, 0.1 mg/mL), and o-phenylenediamine dihydrochloride (OPD) (4.0 μL, 0.5 mg/mL). The sensing enzymes and substrates were loaded on the center of the detection zone. Universal pH indicator solution (0.2 μL) was loaded on the pH detection zone for the measurement of pH. The filter paper changes its visual appearance, darkening, when wetted by sweat that flows in from the inlet to the collection areas.

Photos are acquired at two different stages of the process. First, photos of the wetted patches were taken by a smartphone and analyzed using the ImageJ software to determine the wetted surface area and *L, a, b* value of pH measurement zone. The pH-

View Article Online
DOI: 10.1039/C9LC00734B

value could also be determined by visually matching the color to the standard color set. Secondly, after the patches were air-dried and the colorimetric reactions were completed, photos were again acquired and analyzed by ImageJ to determine the color intensities, which we then used to predict the glucose (pink) or lactate concentrations (yellow).

Sensing of sweat in humans

The experimental approach of human studies were reviewed and approved by the Institutional Review Board for Human Participants at Cornell University with a protocol number of 1804007937. Twelve adult volunteers (10 completed) participated for the perspiration study in a gym with access to drinking water and emergency medical kits. Written consents were obtained from each volunteer before proceeding. We advised the participants to attach the sweat patches on comfortable positions on the participant's hand or arm and to generate sweat (to the marker line in the sweat collection zone, 6.25 μL) for analysis by exercising on treadmills or elliptical machines. Patches were collected and photographed by a smartphone immediately following the workout (lighting uncontrolled). The photos of the patches were used for the determination of sweat loss and pH level. The sweat patches were then placed in petri dishes and air-dried before a second photograph was taken to capture the color intensity on the detection zones. The photos were analyzed by ImageJ software to calculate the wetted area and color intensities. The sweat volume and glucose concentration were calculated based on a standard curve constructed from simulated sweat with various concentrations of glucose. The substances in the sweat stay on the sweat collection zone after the patches are dried. Biomolecules, such as vitamins and other nutrients, were easily extracted by water and subsequently quantified by liquid chromatography-mass

View Article Online
DOI: 10.1039/C9LC00734B

spectroscopy (LC-MS).

Results and discussion

Design and fabrication of the wearable device for sweat monitoring. For the design of our POC wearable sweat capturing/monitoring platform, we took several key features and characteristics into account, including flexibility, comfort, *in situ* monitoring/colorimetric sensing, cost-of-fabrication, and ease of handling for further lab analyses. Our POC wearable sweat biosensor includes four layers. These four layers are assembled together to form a patch that can be mounted on human skin (**Fig. 1a**). The top layer is a transparent adhesive medical tape (**Fig. 1a-i**), which is attached on top of a piece of patterned filter paper (**Fig. 1a-ii**). This transparent tape layer prevents the evaporation of sweat. The patterned Whatman # 1 filter paper was used as the matrix to capture and store sweat due to its flexibility and hydrophilicity. It also serves as the carrier for sensing enzymes and chemicals. The filter paper is extremely lightweight, thin, and also resistant to damage from bending and twisting, making it as an ideal material to wear and adhere closely to the surface of human skin. The third layer, as shown in **Fig. 1a-iii**, is a piece of double-sided medical tape, which is attached to the fabricated pattern (**Fig. 1a-ii**) on one side and to a piece of protective paper (**Fig. 1a-iv**) on the other side. This protective paper can be easily peeled off, allowing the patch to be mounted on human skin *via* the adhesive tape (**Fig. 1a-v**).

Fig. 1b provides more details about the characteristics and functionality of our wearable POC biosensor. The top adhesive tape layer (**Fig. 1b-i**) has two small vents to provide O_2 for the glucose/lactate enzymatic reactions which occur in the underlying glucose and lactate assay zones. As shown in **Fig. 1b-iii**, the double-sided tape layer features

View Article Online
DOI: 10.1039/C9LC00734B

six holes that serve as sweat inlets, labeled 1–6, which allow the sweat from human skin to enter the patterned paper device. The inlets are connected to the assay zones by the channels, which route the sweat from human skin to the detection (circular) and collection/storage (rectangular) zones using capillary force. Inlets #1 and #2 are connected to the two identical rectangular zones, *i.e.* sweat storage/sweat loss detection zone. Inlets #3 and #4 are used to route sweat to two identical pH assay zones. The sweat for the lactate and glucose assay zones are routed using inlets #5 and #6, respectively. As the sweat flows from the inlets to the detection zones, the glucose/lactate is oxidized by the glucose/lactate oxidase, which produces hydrogen peroxide and further oxidizes the pre-loaded color substrates in the presence of peroxidase.[18, 46, 47] Sufficient supply of oxygen is needed for the reactions and is provided *via* the two vents made on top of the transparent layer (**Fig. 1b-i**). **Fig. 1b-ii** also magnifies the lactate and glucose zones in a perspective view to show the alignment of the vents on the top transparent layer with the underlying patterned filter paper. Moreover, **Fig. S1** displays the different device designs that we studied and optimized to reach the current final design described in **Fig. 1**.

In our patch, we designed the channels using computer software and printed the patterns using a solid-phase wax printer (see **Supplementary Movie** and **Fig. S2** for fabrication details). One of the major advantages of this technique is its ability to print hundreds of devices in just a few minutes, making fabrication highly efficient and cost-effective (see **Supplementary Movie)**. This is important because conventional microfluidic devices made out of PDMS *via* well-established soft lithography techniques often require a cleanroom for device fabrication and are limited for large-scale device fabrication. **Fig. 1c** shows images of the front and back sides of the device, including

View Article Online
DOI: 10.1039/C9LC00734B

before (**Fig. 1c-i**) and after (**Fig. 1c-ii**) adding the double-sided medical tape on the back side of the device and the transparent tape on the front side (**Fig. 1c-iii**). After adding the transparent tape on the patch, the features of the device can still be clearly seen, including the channels, assay zones, etc. (**Fig. 1c-iii**). Moreover, **Fig. 1c-iv** shows the two vents aligned to the glucose and lactate assay zones. By peeling off the protective paper on the bottom side of the device, exposing the double-sided tape, the patch can be easily adhered to the surface of human skin (**Fig. 1d**). The double-sided medical tape from 3M is designed to remain adhered for up to 24 h. We also examined the excellent contrast between the wetted storage zone and the rest of the device at different lighting exposures (**Fig. S3**).

Characterization of the channels/assay zones. The key to creating channels/assay zones on filter paper by the wax printing method is that the wax must be fully melted and penetrate through the filter paper to the back side of the substrate. The printing line width (the initial amount of wax) and the temperature are two key factors for controlling the morphology of the melting wax. The printing line width determines how much wax will be printed on the filter paper, while the heating condition determines how much wax can be melted to the back side of the paper. We empirically found that a line width of ~ 380 μm and heating at 170 ˚C for 180 s resulted in ideal microchannel barriers, which can efficiently confine the sweat fluids in channels. Then, after printing the wax on filter paper, we heated the patterned paper on a hot plate for a short period of time (~ 3 min) to melt the wax, allowing the wax to penetrate and reach the back side of the paper (see **Supplementary Movie)**. **Fig. 2a** shows optical images of the patterned filter paper over different heating times (0–180 s), as well. Without any heating, the wax stays on the front side of the filter paper and the back side of the paper remains blank.

Within 30 and 60 s of heating, we observed the wax to penetrate through the filter paper until it reached the back side of the paper device. However, the boundaries of the channels were not fully sealed by the wax. As we extended the heating time, more wax melted and penetrated to the back side of the paper (see **Supplementary Movie)**. Over this time, the wax also spreads horizontally to make the line wider, as shown in the schematic of **Fig. 2a** (wax penetration part). Based on the results obtained, we selected 180 s of heating time to melt the wax and form the channel barriers. After this amount of time, the wax barriers have shown to contain the sweat in channels very well when the volume is less than 12.5 μL (**Fig. S3**). **Fig. 2b** illustrates the comparison between the microscopic morphology of the filter paper before and after heating. The line width increased from ~380 μm to ~880 μm after heating for 180 s, indicating the spreading of the wax on the filter paper. As the wax barriers widen, we found the width of the inlet channels reduced from ~930 μm to ~540 μm. The cellulose fibers on the filter paper do not reveal any morphological changes when examined under an optical microscope, remaining ~15–20 μm in diameter (**Fig. 2b**), as also shown in the scanning electron microscopy image (**Fig. S4**). The 180 s of heating at 170 ˚C also did not alter the physical and mechanical properties of the filter paper. **Fig. 2c** shows that the device can sustain severe bending and twisting, recovering quickly within a few seconds (see **Supplementary Movie**). The flexibility of the paper-based device allows it to easily attach and conform to the surface of skin in a manner (see **Supplementary Movie)** that draws and directs sweat through the patterned channels using the strong capillary force generated by the cellulose fibers of the filter paper (**Fig. S4**) and also by the action of perspiration pressure.

Quantitative analysis of the sweat volume, glucose concentrations, lactate

concentrations, and pH. One of the most important features of our wearable platform is *in situ* measurement of targeted analytes found in sweat. The device features two rectangular zones that are designed to collect/store the sweat and measure the sweat volume, enabling the average sweat rate to be calculated over time. As shown in **Fig. 3a**, the sweat can be easily observed on the sweat collection zone. The wetted area has a remarkable contrast (grey color) compared to other areas (**Fig. S5**). We found a linear relationship between the wetted surface area and the sweat volumes (R^2 = 0.9933), suggesting the wetting area could be used to quantitatively measure the volume of sweat generated from the epidermis. **Fig. 3b** shows the results of the colorimetric reactions induced by adding artificial sweat containing different concentrations of glucose (0–300 μM) through the device inlet. We used ImageJ software to calculate the intensities of the pink color of indicator after the sweat dried. The intensity of the pink color has a strong correlation with the concentration of the glucose (R^2 = 0.9825). It is worth noting that the range of 50–120 μM is especially important because it represents the sweat glucose levels associated with normal blood glucose. Therefore, our wearable patch (biosensor) might potentially be used to predict an acceptable range of blood glucose levels in a non-invasive manner. It is generally considered difficult to achieve a low detection limit of glucose in sweat by colorimetric methods due to the intrinsic limitations of colorimetric sensing. Previous paper-based biosensors have focused on biological fluids other than sweat and reported linear detection ranges of 100 – 1000 μM,[47] 1 – 10 mM,[41] and 2.8−28.0 mM[48] for glucose. We tailored our device and selected a quinone colorant for the glucose detection. We created a vent on the top layer of the device to allow oxygen to be delivered into the glucose detection zone. At the same time, as the water from the sweat evaporates and escapes from the vent, it directs the sweat flow to the venting area and concentrates the glucose and colorants, which greatly

View Article Online
DOI: 10.1039/C9LC00734B

increases the sensitivity of our designed colorimetric sensing for glucose (**Fig. S6**). Without this design, the detection limit of similar devices is as high as 300 μM, which is not sufficient for POC testing of sweat glucose (**Fig. S7**). Our wearable device makes it possible to detect the sweat glucose within the physiological range using color as an indicator *via* the venting/concentrator design (**Fig. 1d** and **Fig. S6**). **Fig. 3c** and **3d** show the measurement of pH and lactate in the artificial sweat. pH is associated with hydration status in human health.[49] For the pH measurement, we used a universal pH indicator solution that changes color from red to yellow between 4.0–7.0. As shown in **Fig. 3c**, we could visually detect the pH change of the artificial sweat based on the color in the pH detection zone. The pH measurements on paper based devices have previously been accomplished by a smartphone-based health accessory.[50] Lactate is a useful marker to predict exercise intolerance, tissue hypoxia, and other metabolism in the human body.[51, 52] The wearable patch is a convenient way to monitor the lactate concentration in sweat for athletes. As shown in **Fig. 3d**, the color density in the lactate detection zone increased as the concentration of lactate increased using o-phenylenediamine dihydrochloride as a color substrate, demonstrating a linear relationship. It is worth noting that the lactate (5 mM), due to its high concentration in sweat, could also be detected by other sensing reactions and designs with/without color concentrated in the venting zone (**Fig. S8**).

Smartphones can be used to capture the photo of the device and acquire quantitative color data for easy home testing. However, one of the biggest challenges for using a smartphone with colorimetric methods for biomolecule quantification is the variation in captured photos caused by different light exposure, camera distance, etc.[53] To eliminate the errors caused by these variations, we studied the glucose standard curves

determined by the actual color intensity (sensing zone), intensity difference ($I_{\text{sensing zone}} - I_{\text{control zone}}$), and the intensity ratio ($I_{\text{sensing zone}} / I_{\text{control zone}}$), when the photo was taken from different distances and lighting exposures (**Fig. S9** and **S10**). To capture a visible photo of our wearable biosensor, the distance from the smartphone camera needs to be adjusted in the range of 3 to 5 inches. We averaged the results obtained from images taken at these distances, and made an averaged standard curve. As shown in **Fig. 4a** and **4b**, the standard curves based on the intensity difference and intensity ratio both show a linear relationship between the values and glucose concentrations. Further, we also compared photos taken from weak, medium, and strong lighting exposures and the corresponding standard curves are shown in **Fig. S10**. The averaged standard curves under different lighting exposures showed linear relationships (**Fig. 4c** and **4d**). However, it seems that the intensity ratio is a better indicator when we compared the R-squared values, slope, and intercept of the averaged standard curve equations at different distances and lighting exposures (Fig. **4b** and **4d**): $Y = 0.0038 X + 1.0798$, $R^2 = 0.9727$, and $Y = 0.0036 X + 1.1218$, $R^2 = 0.9723$. Using the intensity ratio between the glucose sensing zone and the designated control zone (the center of the patch) to quantify the glucose would serve to minimize the errors caused by the variation in cell phone images.

Simulated sweat spiked with certain concentrations of glucose were tested to validate if our method can be used for quantification purposes. As showed in **Table S1**, our POC device coupled with smart phones can successfully quantify the spiked glucose in the simulated sweat. For the spiked concentrations of 0, 50, 200, and 300 μM, our method has calculated the concentration to be -13.79, 67.08, 200.29, and 322.25 μM, respectively. These results indicated that the sensing reactions, the colorimetric

View Article Online
DOI: 10.1039/C9LC00734B

readouts, and the image processing algorithm works well in predicting the concentration of glucose in the sweat and may use as a very convenient and cost-effective method to estimate the concentration of sweat glucose. However, the sensitivity may be improved by using strictly controlled lighting for taking photos, or by using a portable colorimetric device coupled with smart phones. In this way, we may further improve the sensitivity and reduce the standard errors for the measurements at low concentrations (<50 μM).

Correlation between the required amount of sweat and the glucose concentration. Finding the minimum and maximum amounts of sweat required for a consistent and reliable glucose testing assay is crucial for our wearable POC biomarker assay biosensor. **Fig. 5a-i** shows a schematic of the glucose assay zone (including the zone-1 and zone-2 in **Fig. 5a-i**), in which the yellow color represents the loaded and dried glucosidase enzyme. **Fig. 5a-ii** demonstrates the schematically isolated sweat collection zone loaded with "m" volume of sweat during the glucose assay. **Fig. 5A-iii** shows what happens when the "m" volume of sweat is not enough to fully wet zone-1 of the glucose assay (first panel at $t = t_0$). Consequently, the enzymatic reaction is performed only in zone-1 and a light pink color—*i.e.*, the color indicator—appears in the reaction zone (the second panel at $t = t_0$ of **Fig. 5A-iii**). As discussed in the device characterization of **Fig. 1**, we have designed our wearable POC biosensor to feature a vent between glucose assay zone-1 and zone-2 in order to help the water from the collected sweat evaporate more quickly. When the water evaporates from the sweat, the pink color indicator will become more concentrated toward the evaporation direction (see the arrows in **Fig. 5A-iii**). However, due to the dry region between the forefront of the reaction area in zone-1 and the vent (shown as "r_1" on the second panel at $t = t_0$ of

View Article Online
DOI: 10.1039/C9LC00734B

Fig. 5a-iii), the sweat cannot significantly progress toward the vent and concentrate while the water is evaporating (panels $t = t_1$, t_2, and t_3 of **Fig. 5a-iii**, $r_2 < r_1$). This causes the pink-colored indicator to distribute across a wide area and resulting in a color intensity (Intn.) that is variable (vrble). **Fig. 5a-iv** shows a real patch immediately after it was loaded with 1.2 μL of artificial sweat, showing the beginning of the enzymatic reaction (*i.e.*, $t = t_0$) and after the patch has fully-dried (*i.e.*, $t = t_3$). As can be seen on the patch at $t = t_0$, the sweat (1.2 μL) is not enough to fully wet zone-1. After the sweat at the glucose assay zone fully dried ($t = t_3$), the intensity difference (small venting zone to a control zone, **Fig. S9**) was zero and zone-1 itself featured a very weak pink color intensity (**Fig. 5a-iv**, second panel). We also measured the gray value along the zone-1 diameter, namely the screened arrow on the inset of **Fig. 5a-v**, representing the pattern of the indicator after zone-1 is air-dried. The gray value increases along the normalized screening arrow, illustrating an increasingly weak pattern of the dried indicator dye.

We also studied the patterns of the pink-color indicator for other cases, including: (i) sweat that fully wets only zone-1 ("n" volume of sweat loaded, **Fig. 5B**), (ii) sweat that wets (*i.e.*, saturates) both zone-1 and zone-2 ("2n" volume of sweat loaded, **Fig. 5c**), and (iii) sweat that over-saturates both zone-1 and zone-2 with loading of more than "2n" volume of sweat, while the collection sweat is not 100% wetted (**Fig. 5d**). In **Fig. 5b-i**, "n" volume of sweat is loaded into the sweat collection zone. The "n" volume of sweat is enough to only wet the glucose assay zone, as schematically shown using gray color in **Fig. 5b-ii** at $t = t_0$. This amount of sweat causes the enzymatic reaction in assay zone-1 (light pink color), while there is no enzymatic reaction in assay zone-2 (light yellow color in **Fig. 5b-ii**). We also confirmed this fact experimentally using 2.5 μL of 300 μM artificial sweat loaded into the designed POC biomarker assay patch in **Fig.**

5b-ii. Upon subsequent sweat evaporation, the sweat pulls and concentrates the pink-colorant toward the evaporation direction (vent) (shown in **Fig. 5b-iii** schematically at time-points t_1 and t_2 and in the experimental test). When glucose assay zone-1 is fully dried, the indicator dye is concentrated toward the vent and a remarkable intensity of pink-colored indicator appears (**Fig. 5b-iv**). This concentrated indicator is extremely well-aligned with the vent. In this case ("n" volume of collected sweat), we determined that the intensity difference was 40.

If "2n" volume of sweat is collected in the sweat collection zone (**Fig. 5C-i**), it should be sufficient to wet both glucose assay zone-1 and zone-2 (**Fig. 5c-ii**). In this case, the enzymatic reaction occurs in both zones, as shown experimentally in **Fig. 5c-ii**. The water evaporation from sweat in this case ("2n" volume of sweat loading) will occur in a counter-current manner (see the arrows' direction in this figure) and toward the vent, as demonstrated using the arrows in **Fig. 5c-iii**. After concentrating the indicator dye toward the vent, the intensity should be approximately twice that when only "n" volume of sweat was used (**Fig. 5b-iv**), which we confirmed, with an intensity difference of 85 for 5.0 μL of artificial sweat loading in **Fig. 5c-iv**.

If more than "2n" (> 2n) volume of sweat is loaded into the glucose assay zones, however, not 100% wetting the sweat collection zone (**Fig. 5d-i**), the same trends of enzymatic reaction in both zones and the counter-current water evaporation in the glucose assay zones occur (**Fig. 5d-ii**, and **5d-iii**). However, the intensity difference is correlated to the volume of the sweat loaded. In this case (**Fig. 5d**), we loaded 9.0 μL of 300 μM artificial sweat and obtained an intensity difference of 135 (**Fig. 5d-iv**). As a result, to determine the exact concentration of glucose in sweat using our POC biomarker platform, it is necessary to record the initial volume of sweat at $t = t_0$, as

indicated by **Fig. 2** using the wetted area in the sweat collection zone. However, using data processing and dividing the final intensity of the indicator by the initial collected volume of sweat ensures that the obtained intensities are calibrated to the same scale of the sweat volume. Eventually, if more than the storage/collection zone saturation (> ~ 12.5 µl), the sweat is loaded in, we will not be able to calibrate the exact concentration of glucose and consequently the test is failed (not shown here).

Human perspiration study. We tested our wearable POC biosensor on human subjects to verify its sensing functionality and performance. The patches for the human studies were designed to have two glucose sensing zones, two sweat collection/sweat loss sensing zones, and two pH monitoring zones to increase the accuracy of the tests (**Fig. S11**). The human participants were advised to wear the patch while exercising, in order to generate sweat for the study. They were asked to stop the exercise and peel off the patch when the sweat reach the marker line in the sweat sensing zone. Ten participants completed their tasks, generated enough sweat, and returned the patches. Two sets of photos were taken for the patches — one immediately after the exercise and one after the patches had dried. All of the participants reported no discomfort and no interference to their exercise as they were wearing the patches.

Fig. 6a illustrates our wearable patch mounted on the forearm of one of the human participants during workout. The sweat can be seen on the patch inlets in 4 min and more sweat were progressed through the wearable patch as workout continues to 7 min and 13 min. When the sweat reached the marker line in the sweat collection zone at 20 min, the optimal sweat volume has been generated. The workout was stopped and the patch was peeled off from the participant's forearm for drying. The air-dried patch and the magnified glucose detection zone are also shown in **Fig. 6a**. The pink color

developed due to the presence of sweat glucose and concentrated in the venting area, as shown in the magnified glucose detection zone, can be easily seen by eyes without using any additional instrument.

As shown in **Fig. 6b**, the wearable patches successfully directed the sweat from the human epidermis to the sweat collection and detection zones for the 10 human subjects. The hydrophobic wax barrier can contain the sweat in the channels with minimum leakage (**Fig. 6b**). One of the functions of the device is to monitor the volume of sweat that is generated during exercise. All of the subjects can successfully generate sweat for the study and most of them can reach the optimal sweat level as showed in the sweat monitoring/storage area (**Fig. 6b**). There was sufficient contrast between the wetted sweat collection area (rectangles) and the dry areas, which made it possible to quantify the volume of sweat based on the area of the wetted zone (**Table 1**). We were also able to read the pH value visually when compared to the standard colors shown in **Fig. 3C**. The pH measurement here, performs like pH (litmus) paper and serves to indicate the pH of sweat (**Table 1**).

Photos were also taken after the patches were air-dried. As shown in **Fig. 6b**, the pink color appears in the glucose detection zones, with subjects 1, 7, and 9 showing the strongest pink color. The color intensity ratio of the glucose detection zones and the designated control zone (center of the patch) were determined by software and used to predict the glucose concentration in the sweat. **Table 1** shows the glucose concentration in sweat from different subjects before and after corrected by the sweat rate. We observed glucose concentrations between 4.7 and 98.4 μM for eight of the subjects, which is in the normal range of sweat glucose (<120 μM).[54] Subject 2 and 10 have a relatively high sweat glucose concentration of 163.5 μM and 336.1 μM, respectively.

The high glucose readout in subject 10, corrected by the sweat volume, could potentially indicate a prediabetic or diabetic condition for the subject. This result could serve as a first alarm to the subjects and prompt further in-lab confirmation of conditions. The goal of designing this POC biosensor is to help monitor the glucose or diagnose the hidden prediabetes and diabetes conditions with convenience, minimal invasions, and affordable cost.[54]

Moreover, the sweat contains rich information concerning human nutrition. The dried sweat samples stored on the patches were re-extracted by water and analyzed using LC-MS. The results showed that we can successfully detect a range of biomarkers in the sweat, including creatine, lactate, choline, and several B-vitamins (**Table S2**). The patch provides a convenient way to collect sweat, store the biomarkers, and mail for lab analysis. The patches are affordable and can be used daily or weekly to monitor changes in targeted biomarkers found in sweat. Such information could be used to detect nutritional deficiencies and personalize nutritional intakes (*e.g.* micronutrients).

In summary, we designed a versatile, cost-effective, flexible, wearable device for sweat collection and monitoring in this study. The device can detect sweat loss, pH, glucose concentrations and lactate concentrations in sweat, with the ability to detect glucose levels in the physiological range of 50–300 μM. This cost-effective, wearable, patch could potentially provide instant concentration results for biomolecular targets of interests if coupled with the imaging and computing capabilities of a smartphone. Meanwhile, the wearable patch could potentially be used to collect information for personalized nutrition or medicine.

REFERENCES:

1. M. N. Sawka and C. B. Wenger, *Physiological responses to acute exercise-heat stress*, ARMY RESEARCH INST OF ENVIRONMENTAL MEDICINE NATICK MA, 1988.
2. K. Hooton, W. Han and L. Li, *Analytical chemistry*, 2016, **88**, 7378-7386.
3. J. Moyer, D. Wilson, I. Finkelshtein, B. Wong and R. Potts, *Diabetes technology & therapeutics*, 2012, **14**, 398-402.
4. F. Herrmann and L. Mandol, *Journal of Investigative Dermatology*, 1955, **24**, 225-246.
5. M. Harker, H. Coulson, I. Fairweather, D. Taylor and C. A. Daykin, *Metabolomics*, 2006, **2**, 105-112.
6. H. Lee, C. Song, Y. S. Hong, M. S. Kim, H. R. Cho, T. Kang, K. Shin, S. H. Choi, T. Hyeon and D.-H. Kim, *Science Advances*, 2017, **3**, e1601314.
7. J. Kim, A. S. Campbell, B. E.-F. de Ávila and J. Wang, *Nature Biotechnology*, 2019, **37**, 389-406.
8. T. Q. Trung and N.-E. Lee, *Advanced Materials*, 2016, **28**, 4338-4372.
9. C. Gisolfi, *Nutritional Needs in Hot Environments: Applications for Military Personnel in Field Operations, Committee on Military Nutrition Research, Institute of Medicine*, 1993, 87-96.
10. L.-C. Tai, W. Gao, M. Chao, M. Bariya, Q. P. Ngo, Z. Shahpar, H. Y. Y. Nyein, H. Park, J. Sun, Y. Jung, E. Wu, H. M. Fahad, D.-H. Lien, H. Ota, G. Cho and A. Javey, *Advanced Materials*, 2018, **30**, 1707442.
11. A. Tricoli, N. Nasiri and S. De, *Advanced Functional Materials*, 2017, **27**, 1605271.
12. G. Mullard, University of Nottingham, 2012.
13. M. Kerr and D. Snow, *American journal of veterinary research*, 1983, **44**, 1571-1577.
14. L. McCutcheon, R. Geor, M. J. HARE, G. L. ECKER and M. Lindinger, *Equine Veterinary Journal*, 1995, **27**, 153-157.
15. E. Vargas, H. Teymourian, F. Tehrani, E. Eksin, E. Sánchez-Tirado, P. Warren, A. Erdem, E. Dassau and J. Wang, *Angewandte Chemie International Edition*, 2019, **58**, 6376-6379.
16. E. Waltz, *Nature Biotechnology*, 2019, **37**, 340-344.
17. T. Wang, H. Yang, D. Qi, Z. Liu, P. Cai, H. Zhang and X. Chen, *Small*, 2018, **14**, 1702933.
18. X. Wang, F. Li, Z. Cai, K. Liu, J. Li, B. Zhang and J. He, *Analytical and bioanalytical chemistry*, 2018, **410**, 2647-2655.
19. J. Kim, J. R. Sempionatto, S. Imani, M. C. Hartel, A. Barfidokht, G. Tang, A. S. Campbell, P. P. Mercier and J. Wang, *Advanced Science*, 2018, **5**, 1800880.
20. A. J. Bandodkar, P. Gutruf, J. Choi, K. Lee, Y. Sekine, J. T. Reeder, W. J. Jeang, A. J. Aranyosi, S. P. Lee, J. B. Model, R. Ghaffari, C.-J. Su, J. P. Leshock, T. Ray, A. Verrillo, K. Thomas, V. Krishnamurthi, S. Han, J. Kim, S. Krishnan, T. Hang and J. A. Rogers, *Science Advances*, 2019, **5**, eaav3294.
21. J. T. Reeder, J. Choi, Y. Xue, P. Gutruf, J. Hanson, M. Liu, T. Ray, A. J. Bandodkar, R. Avila, W. Xia, S. Krishnan, S. Xu, K. Barnes, M. Pahnke, R. Ghaffari, Y. Huang and J. A. Rogers, *Science Advances*, 2019, **5**, eaau6356.
22. J. Kim, I. Jeerapan, J. R. Sempionatto, A. Barfidokht, R. K. Mishra, A. S. Campbell, L. J. Hubble and J. Wang, *Accounts of Chemical Research*, 2018, **51**, 2820-2828.
23. C. W. Bae, P. T. Toi, B. Y. Kim, W. I. Lee, H. B. Lee, A. Hanif, E. H. Lee and N.-E. Lee, *ACS Applied Materials & Interfaces*, 2019, **11**, 14567-14575.
24. S. B. Kim, K. Lee, M. S. Raj, B. Lee, J. T. Reeder, J. Koo, A. Hourlier-Fargette, A. J. Bandodkar, S. M. Won, Y. Sekine, J. Choi, Y. Zhang, J. Yoon, B. H. Kim, Y. Yun, S. Lee, J. Shin, J. Kim, R. Ghaffari and J. A. Rogers, *Small*, 2018, **14**, 1802876.
25. J. Choi, A. J. Bandodkar, J. T. Reeder, T. R. Ray, A. Turnquist, S. B. Kim, N. Nyberg, A. Hourlier-Fargette, J. B. Model, A. J. Aranyosi, S. Xu, R. Ghaffari and J. A. Rogers, *ACS Sensors*, 2019, **4**, 379-388.
26. A. K. Yetisen, J. L. Martinez-Hurtado, B. Ünal, A. Khademhosseini and H. Butt, *Advanced Materials*, 2018, **30**, 1706910.

27. Y. Chen, S. Lu, S. Zhang, Y. Li, Z. Qu, Y. Chen, B. Lu, X. Wang and X. Feng, *Science Advances*, 2017, **3**, e1701629.
28. Y. Lei, W. Zhao, Y. Zhang, Q. Jiang, J.-H. He, A. J. Baeumner, O. S. Wolfbeis, Z. L. Wang, K. N. Salama and H. N. Alshareef, *Small*, **0**, 1901190.
29. P. T. Toi, T. Q. Trung, T. M. L. Dang, C. W. Bae and N.-E. Lee, *ACS Applied Materials & Interfaces*, 2019, **11**, 10707-10717.
30. A. Furniturewalla, M. Chan, J. Sui, K. Ahuja and M. Javanmard, *Microsystems & Nanoengineering*, 2018, **4**, 20.
31. S. Imani, A. J. Bandodkar, A. M. V. Mohan, R. Kumar, S. Yu, J. Wang and P. P. Mercier, *Nature Communications*, 2016, **7**, 11650.
32. E. Bihar, S. Wustoni, A. M. Pappa, K. N. Salama, D. Baran and S. Inal, *npj Flexible Electronics*, 2018, **2**, 30.
33. A. Martín, J. Kim, J. F. Kurniawan, J. R. Sempionatto, J. R. Moreto, G. Tang, A. S. Campbell, A. Shin, M. Y. Lee, X. Liu and J. Wang, *ACS Sensors*, 2017, **2**, 1860-1868.
34. F. Zhang, J. M. Carothers and J. D. Keasling, *Nature Biotechnology*, 2012, **30**, 354.
35. A. Koh, D. Kang, Y. Xue, S. Lee, R. M. Pielak, J. Kim, T. Hwang, S. Min, A. Banks and P. Bastien, *Science translational medicine*, 2016, **8**, 366ra165-366ra165.
36. X. Chen, J. Chen, F. Wang, X. Xiang, M. Luo, X. Ji and Z. He, *Biosensors and Bioelectronics*, 2012, **35**, 363-368.
37. J. Park, J. Kim, S.-Y. Kim, W. H. Cheong, J. Jang, Y.-G. Park, K. Na, Y.-T. Kim, J. H. Heo, C. Y. Lee, J. H. Lee, F. Bien and J.-U. Park, *Science Advances*, 2018, **4**, eaap9841.
38. S. R. Krishnan, T. R. Ray, A. B. Ayer, Y. Ma, P. Gutruf, K. Lee, J. Y. Lee, C. Wei, X. Feng, B. Ng, Z. A. Abecassis, N. Murthy, I. Stankiewicz, J. Freudman, J. Stillman, N. Kim, G. Young, C. Goudeseune, J. Ciraldo, M. Tate, Y. Huang, M. Potts and J. A. Rogers, *Science Translational Medicine*, 2018, **10**, eaat8437.
39. M. Bariya, H. Y. Y. Nyein and A. Javey, *Nature Electronics*, 2018, **1**, 160-171.
40. J. Choi, R. Ghaffari, L. B. Baker and J. A. Rogers, *Science Advances*, 2018, **4**, eaar3921.
41. W.-J. Zhu, D.-Q. Feng, M. Chen, Z.-D. Chen, R. Zhu, H.-L. Fang and W. Wang, *Sensors and Actuators B: Chemical*, 2014, **190**, 414-418.
42. Y. Temiz, R. D. Lovchik, G. V. Kaigala and E. Delamarche, *Microelectronic Engineering*, 2015, **132**, 156-175.
43. E. Carrilho, A. W. Martinez and G. M. Whitesides, *Analytical chemistry*, 2009, **81**, 7091-7095.
44. W. Dungchai, O. Chailapakul and C. S. Henry, *Analyst*, 2011, **136**, 77-82.
45. Y. Lu, W. Shi, J. Qin and B. Lin, *Analytical chemistry*, 2009, **82**, 329-335.
46. Y. Yang, E. Noviana, M. P. Nguyen, B. J. Geiss, D. S. Dandy and C. S. Henry, *Analytical chemistry*, 2016, **89**, 71-91.
47. E. F. Gabriel, P. T. Garcia, T. M. Cardoso, F. M. Lopes, F. T. Martins and W. K. Coltro, *Analyst*, 2016, **141**, 4749-4756.
48. K. Abe, K. Suzuki and D. Citterio, *Analytical chemistry*, 2008, **80**, 6928-6934.
49. J. Chycki, T. Zając, A. Maszczyk and A. Kurylas, *Biology of sport*, 2017, **34**, 255.
50. V. Oncescu, D. O'Dell and D. Erickson, *Lab on a Chip*, 2013, **13**, 3232-3238.
51. L. W. Andersen, J. Mackenhauer, J. C. Roberts, K. M. Berg, M. N. Cocchi and M. W. Donnino, 2013.
52. M. Adeva-Andany, M. López-Ojén, R. Funcasta-Calderón, E. Ameneiros-Rodríguez, C. Donapetry-García, M. Vila-Altesor and J. Rodríguez-Seijas, *Mitochondrion*, 2014, **17**, 76-100.
53. G. G. Morbioli, T. Mazzu-Nascimento, A. M. Stockton and E. Carrilho, *Analytica chimica acta*, 2017, **970**, 1-22.
54. H. Lee, T. K. Choi, Y. B. Lee, H. R. Cho, R. Ghaffari, L. Wang, H. J. Choi, T. D. Chung, N. Lu and T. Hyeon, *Nature nanotechnology*, 2016, **11**, 566-572.

573

View Article Online
DOI: 10.1039/C9LC00734B

View Article Online
DOI: 10.1039/C9LC00734B

ACKNOWLEDGEMENTS:

Special thanks are given to our volunteers for their participation in the study.

CONFLICT OF INTEREST:

The authors declare no conflict of interest.

AUTHORS CONTRIBUTION:

A.A., Z.Z., M.A., M.L. and P.D. conceived and planned the experiments. Z.Z., M.A., M.L., P.D. and P.L. carried out the experiments. A.A., Z.Z., M.A., M.L., P.D. and P.L. contributed to the interpretation of the results. A.A., Z.Z., M.A. and P.D. took the lead in writing the manuscript. All authors provided critical feedback and helped shape the research, analysis and manuscript.

Fig. 1. Schematic design of the wearable device for sweat collection and bio-sensing. **(a)** Schematic illustration of the wearable POC device layers, including the (i) top transparent adhesive layer, (ii) the pattern supported on filter paper, (iii) the double-sided medical tape, and (iv) a protective piece paper, which when fully assembled can serve as a patch that can be mounted on (v) human skin. (**b**) The device functionality in more detail, including: (i) two vents on the transparent adhesive layer for enzymatic O_2 delivery for the glucose and lactate oxidation reactions; (ii) the full design for collecting sweat and monitoring pH, glucose, and lactate, all supported on filter paper (the magnified inset illustrates the glucose detection zone and cross-sectional view of the design); (iii) the double-sided tape; and (iv) the protective paper. (**c**) Images of the device (Diameter: 3.9 cm) before and after the addition of the transparent and medical tape layers, along with a magnified image of the glucose detection zone. (**d**) Image of the wearable device attached on a human hand.

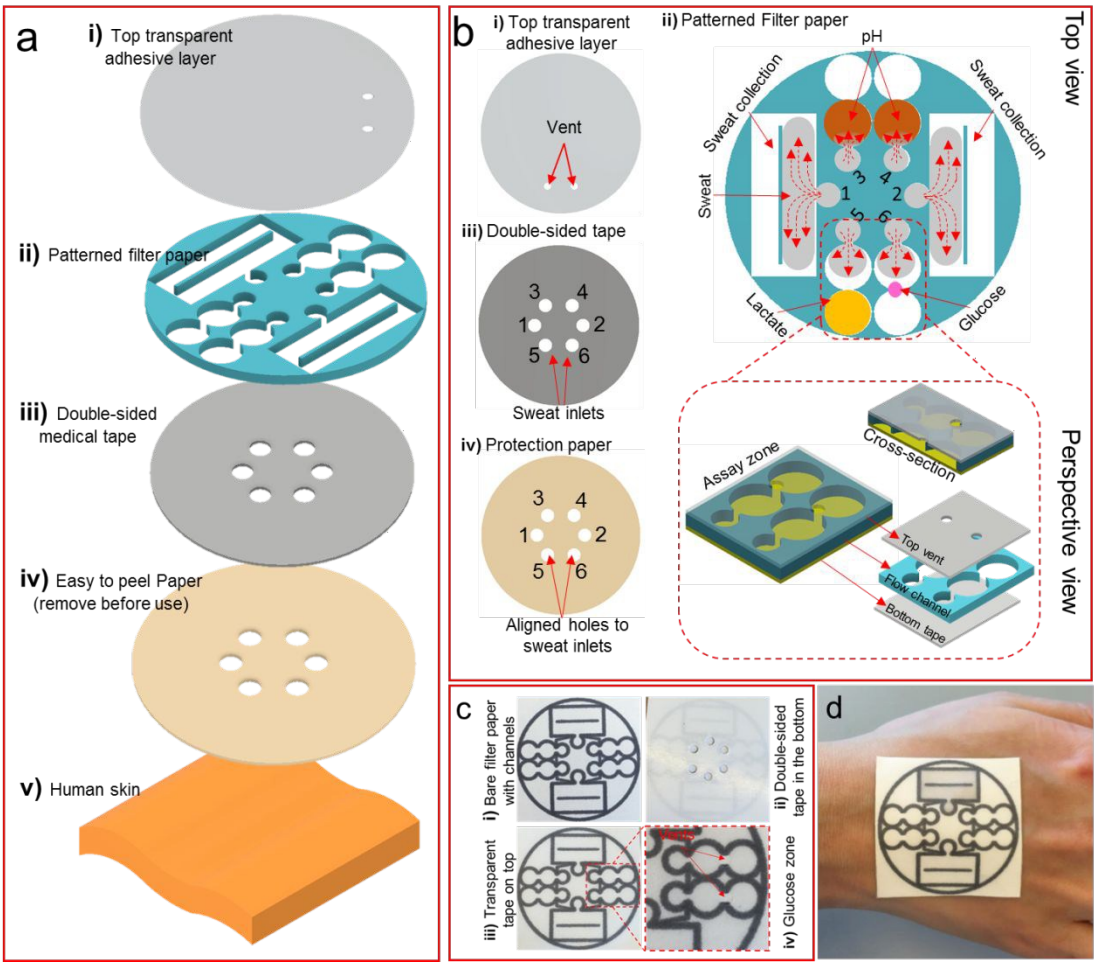

Fig. 2. Characterization of the wax melting process and the flexibility of the wearable device. (a) Front and back side images of the wax-printed filter paper as the device (Diameter: 3.9 cm) was heated over time (0–180 s), and a schematic illustration of the wax penetration process. (**b**) Optical microscopy images of the printed barrier lines and channels, before and after heating. (**c**) Optical images of the wearable device during different handling situations, and its recovered status after severe bending.

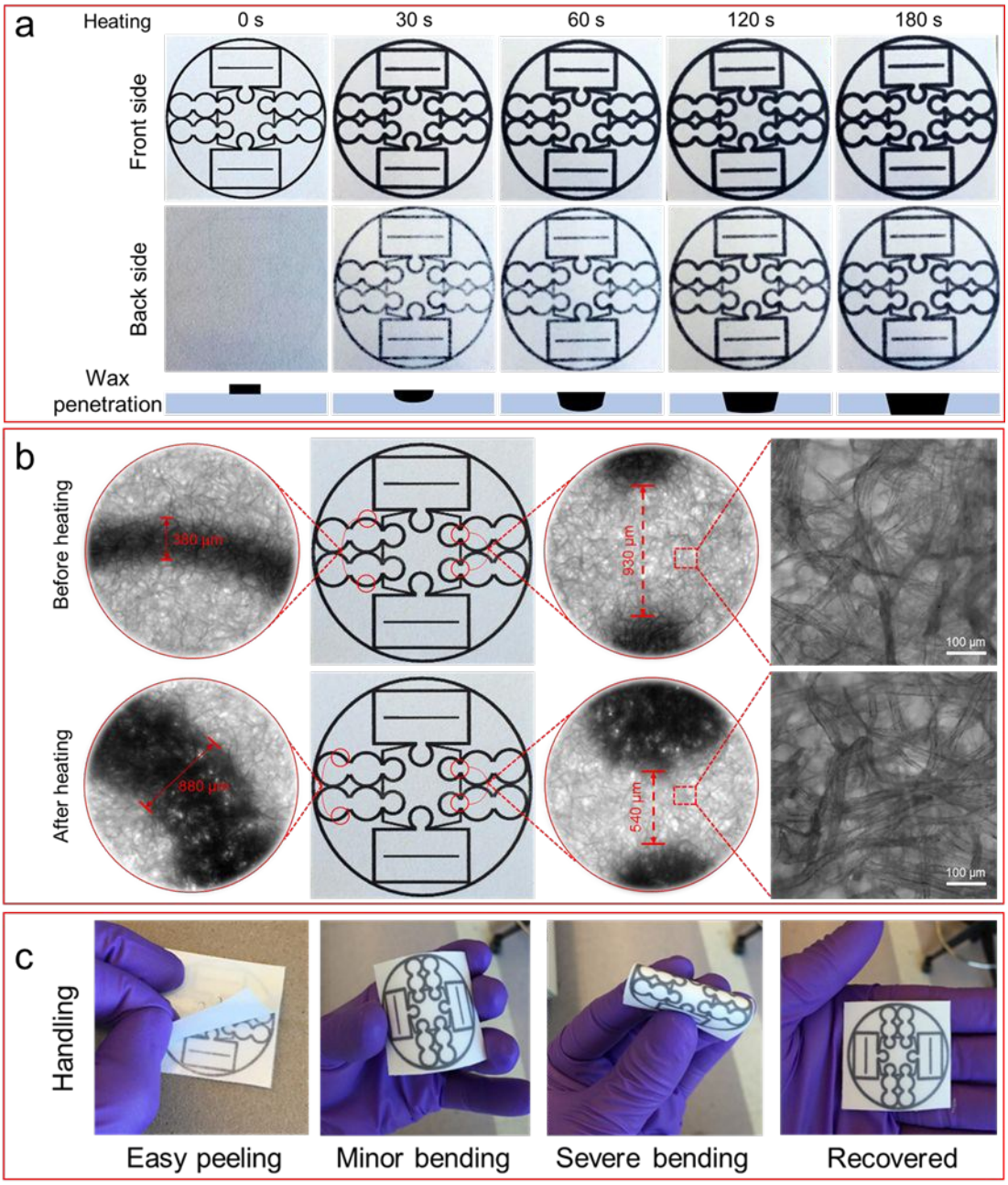

Fig. 3. Detection of the sweat volume, glucose, pH, and lactate by the wearable device. (**a**) Images of the wearable patch (Diameter: 3.9 cm) filled with different volumes of simulated sweat and the wet area analysis. (**b**) Images of the glucose detection zone after exposure to different concentrations of glucose and the analysis of the color intensities. (**c**) Images of the pH detection zone after exposure to simulated sweat with different pH values and the analysis of the color (R, G, B). (**d**) Images of the lactate detection zone after exposure to simulated sweat with different lactate concentrations and the analysis of the color intensities.

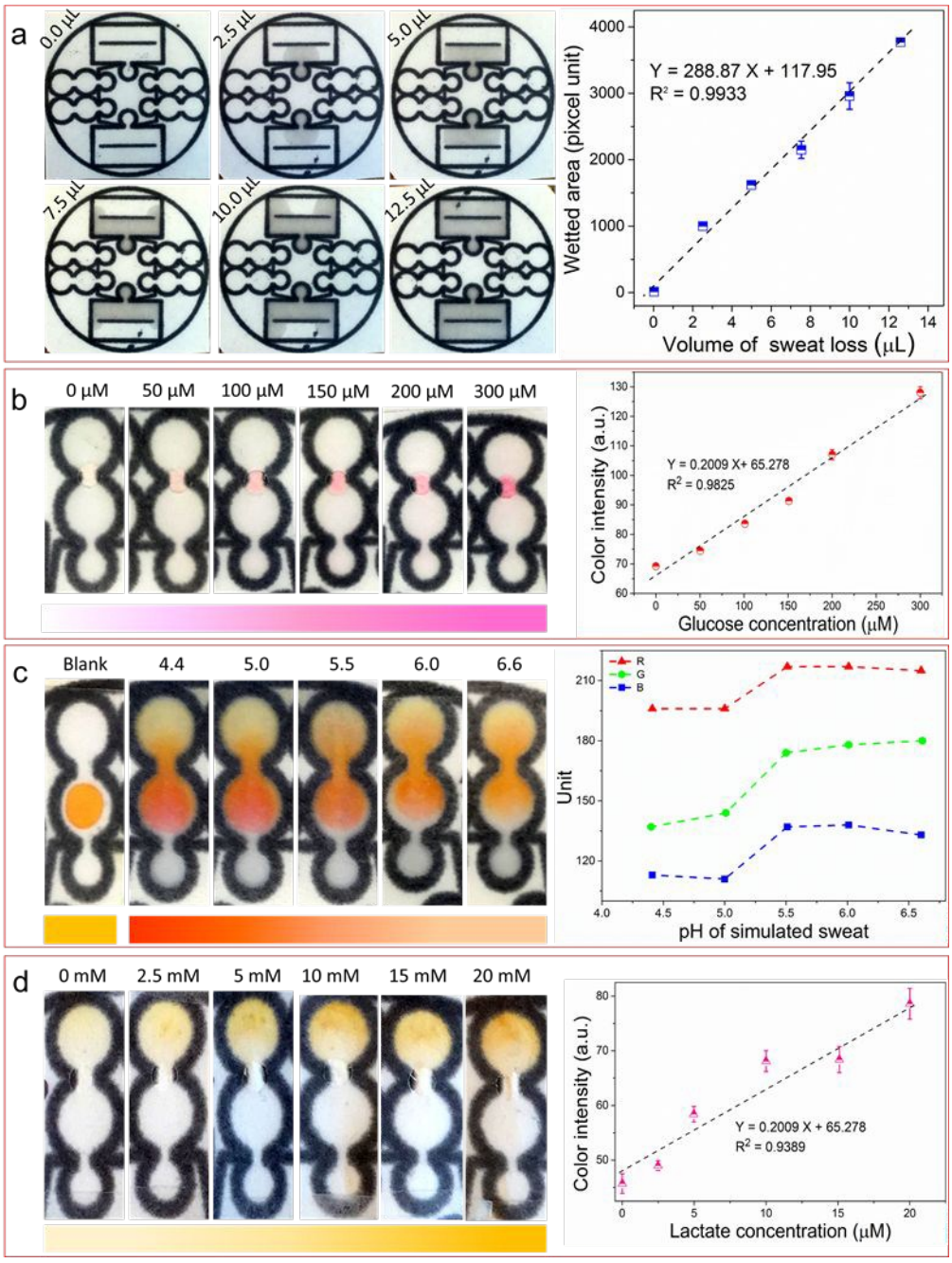

View Article Online
DOI: 10.1039/C9LC00734B

Fig. 4. Quantification of glucose in the sweat: (**A**) Averaged glucose standard curve determined by the intensity difference between the glucose sensing zone and the center of the wearable patch (control) when photos were taken from 3-inch, 4-inch, and 5-inch distances. (**B**) Averaged glucose standard curve determined by the intensity ratio of the glucose sensing zone and the center of the wearable patch (control) when the photos were taken from 3-inch, 4-inch, and 5-inch distances. (**C**) Averaged glucose standard curve determined by the intensity difference of the glucose sensing zone and the center of the wearable patch (control) when the photos were taken from weak, medium, and strong lighting conditions. (**D**) Averaged glucose standard curve determined by the intensity ratio of the glucose sensing zone and the center of the wearable patch (control) when the photos were taken from weak, medium, and strong lighting conditions.

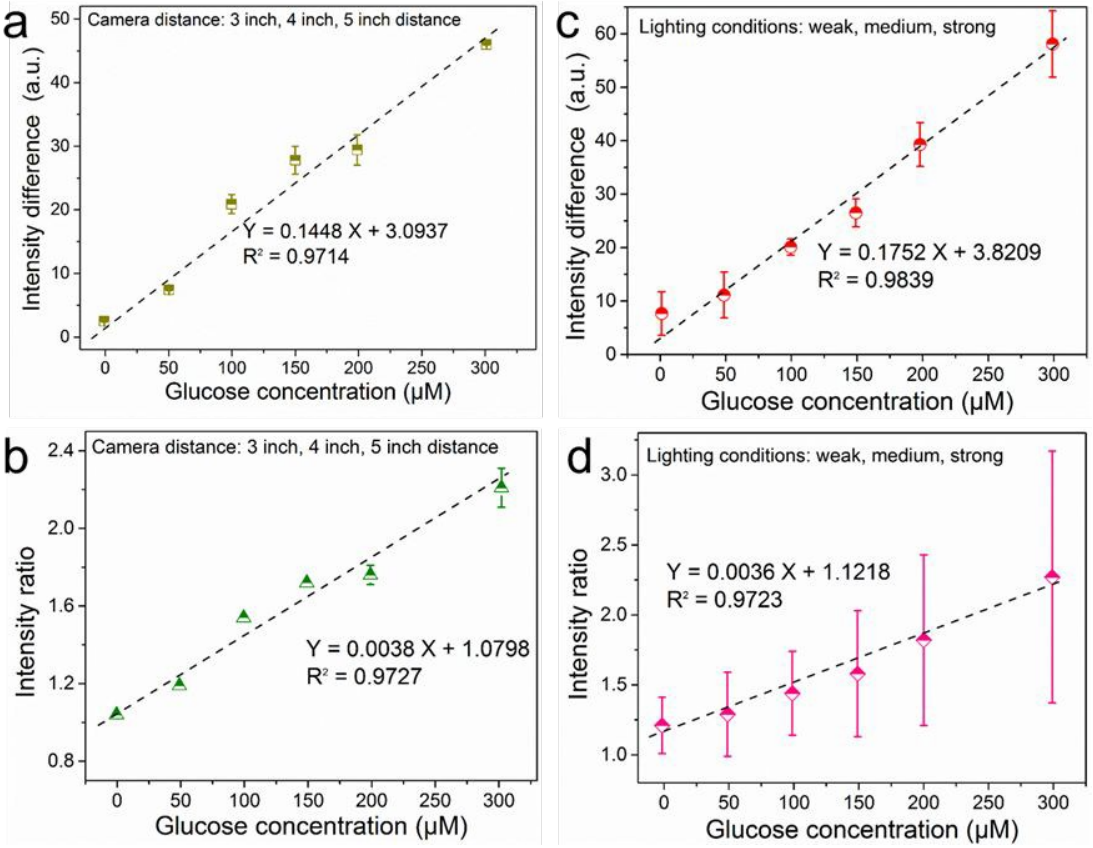

Fig. 5. Correlation between the volume of collected sweat and the intensity of the indicator representing the glucose enzymatic reaction. The device response when the collected volume of sweat is (a) not enough to fully wet assay zone-1 (part "a" includes a schematic glucose assay zone (i), sweat collection and monitoring zone (ii), schematic glucose zone right after workout (t_0) and time-lapse drying (t_1, t_2, and t_3) (iii), two real patches after workout (t_0) and after fully air-dried (t_3) (iv), and the color intensity of the indicator along the screening arrow shown on inset figure (v). The device response when the collected volume of sweat are (b) sufficient to only wet assay zone-1, (c) enough to fully wet assay zone-1 and zone-2 but not over-saturate, and (d) more than enough to over saturate the assay zone-1 and zone-2, but not fully filling the rectangular sweat collection zone. In parts b–d, they include sweat collection and monitoring zone (i), schematic glucose zone and a real tested patch right after workout (t_0) (ii), schematically time-lapse air-drying of the glucose zone (t_1, t_2) and the air-drying real tested patch (t_2) (iii), and fully air-dried schematic glucose zone and a real tested patch (iv).

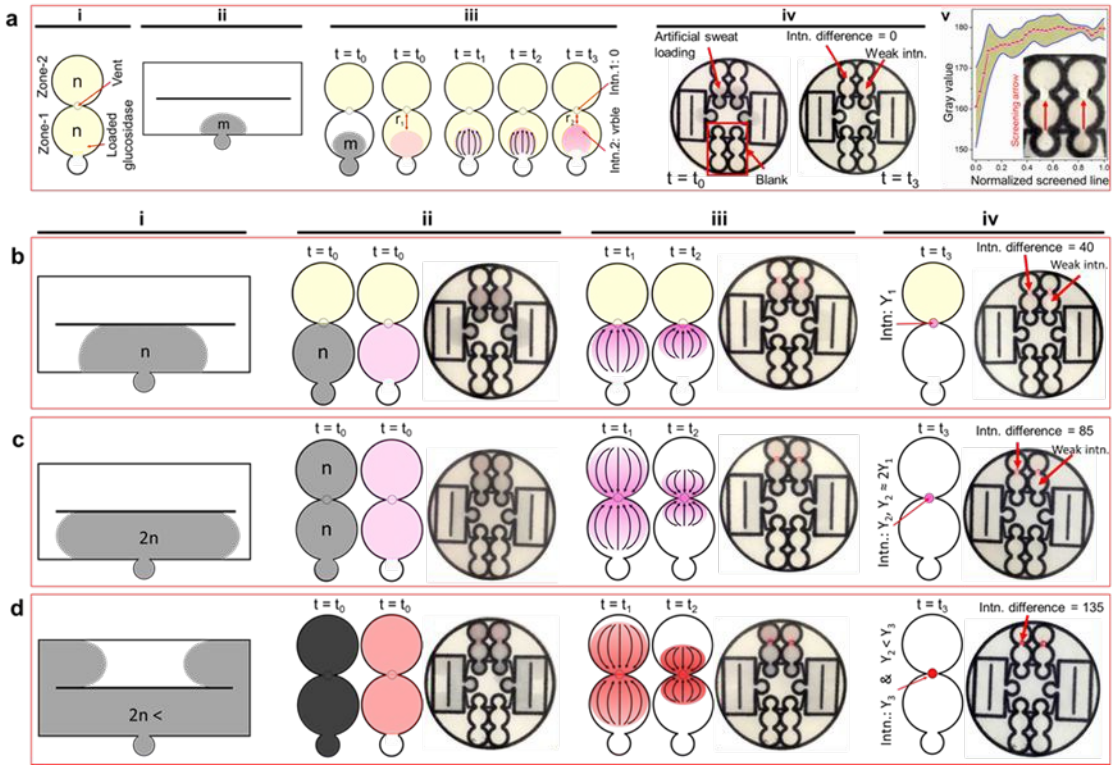

View Article Online
DOI: 10.1039/C9LC00734B

Fig. 6. Use of wearable patches to collect sweat and monitor different biomarkers (glucose and pH) for human subjects during exercise. (a), the device (Diameter: 3.9 cm) attached on a human forearm during exercise at different time and the image of the device after drying; **(b)**, The photos of the devices were taken immediately after the workout and after the patches had air-dried.

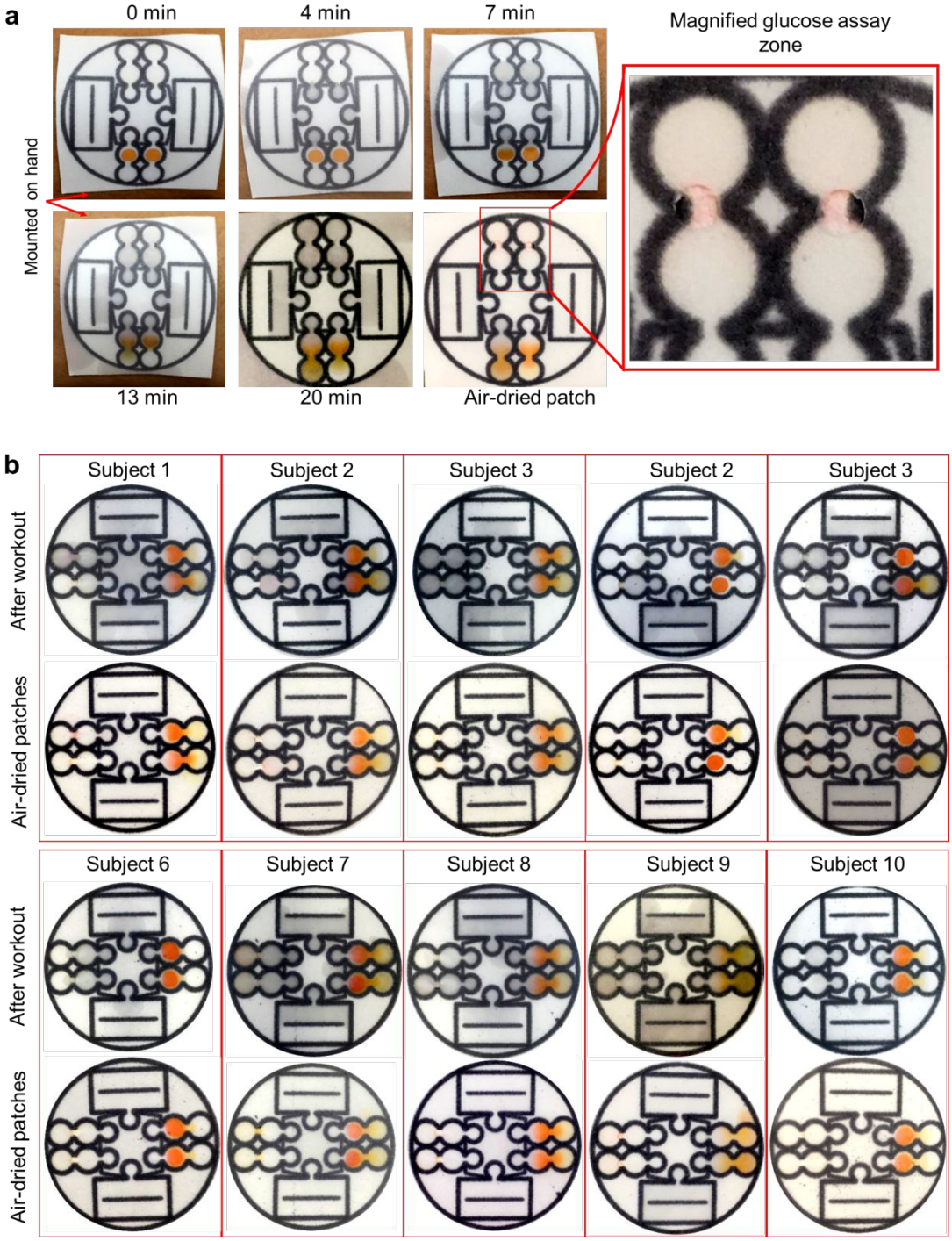

View Article Online
DOI: 10.1039/C9LC00734B

Table 1. The sweat volume, concentration of glucose, and the estimated sweat pH predicted by the sweat patch for the 10 human subjects.

Subject #	Sweat generated (μL)	Con. of glucose (μM)	Con. of glucose correlated by sweat volume (μM)*	Estimated pH
1	7.2	94.4	98.4	5
2	4.1	88.4	163.5	4.4
3	7.7	41.8	40.5	5.5
4	5.6	72.3	96.2	5
5	9.8	32.0	24.5	4.4
6	2.7	1.7	4.7	5
7	7.8	47.6	45.9	4.4
8	6.6	9.6	11.0	5
9	11.2	138.1	92.4	>6.6
10	1.5	68.7	336.1	5.5

*The glucose standard curve was generated using 7.5 μL of simulated sweat with various glucose concentrations. Thus, the concentration of glucose in human subjects was corrected by the volume of the sweat.

668

Graphical Abstract

669

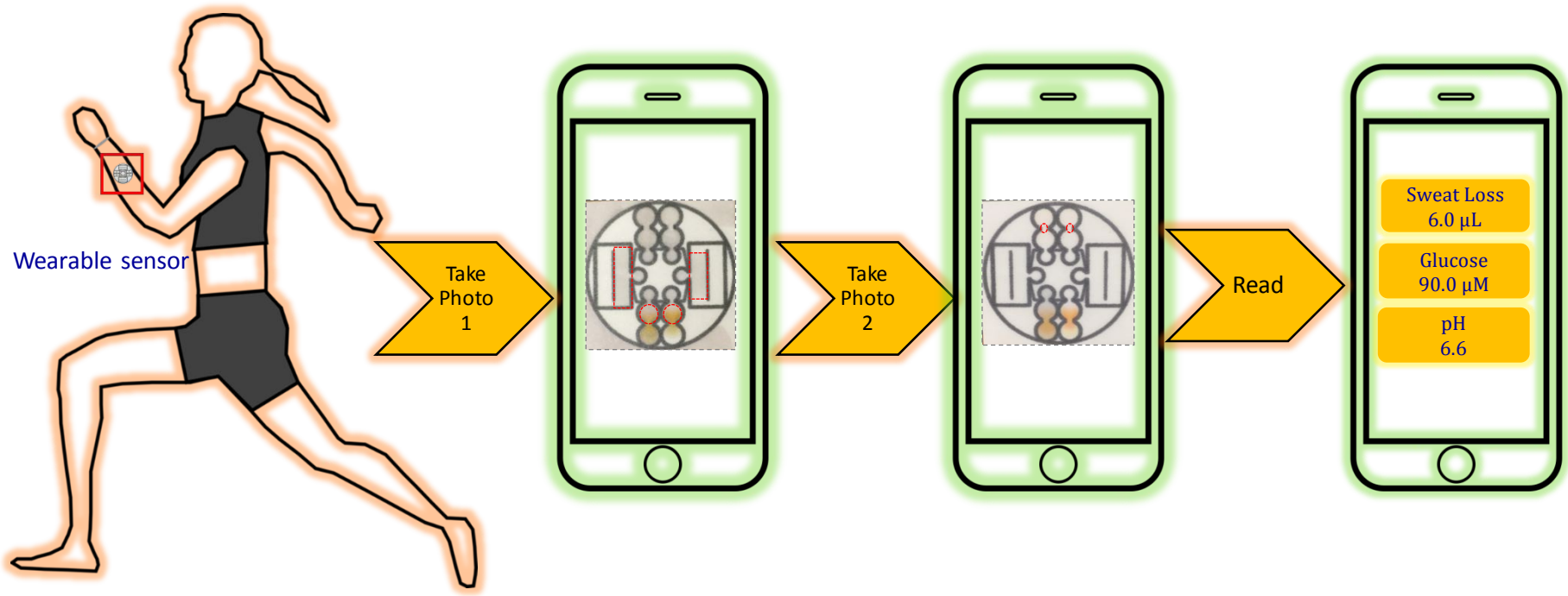

670

671

672

Graphical Abstract 2

673